

Collision Induced Transitions Between Zeeman Substates of Laser Excited Sodium Atoms in Very High Magnetic Fields

J.-C. Gay and W.B. Schneider

Laboratoire de Spectroscopie Hertzienne de l'ENS (Associé au CNRS (LA No 18))
et Université Paris VII, Paris, France

Received April 3; Revised Version June 14, 1976

This is a report on a new method of measuring cross sections for the collision induced population transfer between single Na- $3p\ ^2P$ fine structure Zeeman states. The experiments are done for the five inert gases at the magnetic field strengths of 6, 17, 24, and 51 kOe. From the optically excited $^2P_{3/2, \pm 3/2}$ and $^2P_{1/2, \pm 1/2}$ states, respectively, the transfer to the other Zeeman states is studied. The method allows the determination of cross sections for which the influence of the magnetic field is cancelled and which render possible the calculation of cross sections for the transfer and the relaxation of all 2P density tensor components of the degree $k=1, 2,$ and 3 . The comparison with previous theoretical and experimental results gives satisfactory agreement. As an application the six Grawert parameters are deduced for the inert gases.

1. Introduction

The usual method to study collision induced depolarization of atomic states is the optical measurement of respective multipole relaxation or transfer rates [1]. This method, however, only gives complete information about collision processes for states with $j \leq 1$, i.e. states for which all multipoles are detectable by the emitted light. In the case of alkali-inert gas collisions it is e.g. not possible to measure the octupole relaxation rate in the $^2P_{3/2}$ state. This would be, however, of interest for testing various theoretical predictions concerning fine structure depolarization (for a review see Nikitin 1971, 1974, and 1975, Omont 1976 [2–5]).

Another way [2, 6] to study collision induced depolarization of alkali 2P states is the determination of population transfer rates between 2P Zeeman states. Formerly this method was restricted to the rare cases where the initial and final Zeeman states are discernible by the different polarization of their fluorescent light [7, 8].

To overcome these restrictions we applied a strong magnetic field to achieve a sufficient splitting of the 2P Zeeman states, so that the photons of different Zeeman transitions could be separated energetically.

In this paper we report the application of this method on the case of sodium-inert gas collisions where

sodium atoms are excited to one of the $3p\ ^2P$ Zeeman states. Furthermore we report measurements of the magnetic field dependence of the population transfer rates between single Zeeman states in a magnetic field ranging up to 51 kOe.

2. Experimental

To achieve a sufficient splitting of the Na $3p\ ^2P$ Zeeman states and to decouple the nuclear spin we used a superconducting magnet with a maximum field strength of about 80 kOe. To give an idea of the corresponding energy splitting we give in Figure 1 the respective Zeeman pattern for sodium.

The excitation of a single Zeeman state was performed by a tunable jet stream dye laser whose bandwidth and power were reduced to 0.13 cm^{-1} and 40 mW, respectively. The linewidth of one Zeeman component is 0.095 cm^{-1} at 450 K due to Doppler broadening and hyperfine interaction. Shortterm frequency instabilities caused by mode competition ensured a quasi "white" excitation of the Zeeman state during the integration time of the detection system. To separate the Zeeman components we used a piezo-electrically scanned Fabry-Pérot interferometer with adjustable mirror spacing. The free spectral range of

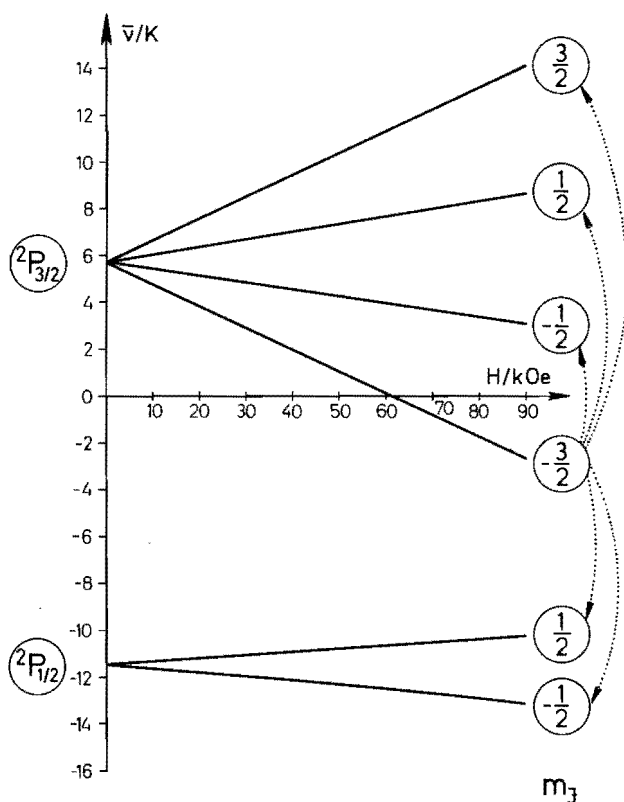


Fig. 1. Zeeman fine structure pattern for the Na $3p^2P$ state in the magnetic field range from zero to 90 kOe

the interferometer was appropriately chosen to get the least overlap of the six $3p^2P$ Zeeman components for various magnetic field strengths. Measurements were made at 6, 17, 24, and 51 kOe. For this the most suitable free spectral range was found to be 2.65 cm^{-1}

(see Fig. 2). To get a sufficient longterm stability ($\geq 3 \text{ h}$) the interferometer was placed in a thermostabilized box. This ensured a constant interferometer function during the measurements.

The arrangement of the apparatus is shown in Figure 3. In designing the experimental arrangement we took account of the principal methods of fluorescence investigations [9]. The technical difficulty was to arrange the oven with its components in the relatively small bore of the magnet. The clear bore was 69 mm which was reduced to 50 mm by an indispensable cooling and isolating system, which kept the bore at room temperature and the inner part of the oven at 450 K. The side arm of the resonance cell with the metallic sodium was kept at the constant temperature of 380 K by an oil circulating system which was connected to an external thermostat.

The excitation of the sodium vapour was performed with the chopped laser beam whose direction was parallel to the magnetic field. The emitted light was deflected by a mirror and then passed through a Glan-type polarizer and a 3 m light guide to the interferometer. With the polarizer we suppressed the π -fluorescence components which give no further information on the collision process. This reduced the number of D_1 and D_2 Zeeman components which we had to resolve to six. The σ -components were recorded by means of the indicated collimator, the photomultiplier, the lock-in amplifier, and the X-Y-recorder. As a function of the inert gas pressure we measured the direct and sensitized fluorescence for both initial $^2P_{3/2, \pm 3/2}$, $^2P_{1/2, \pm 1/2}$ -excitation. $^2P_{3/2, \pm 3/2}$ excitation is most favourable because of the absence of direct optical pumping and because of the relatively large

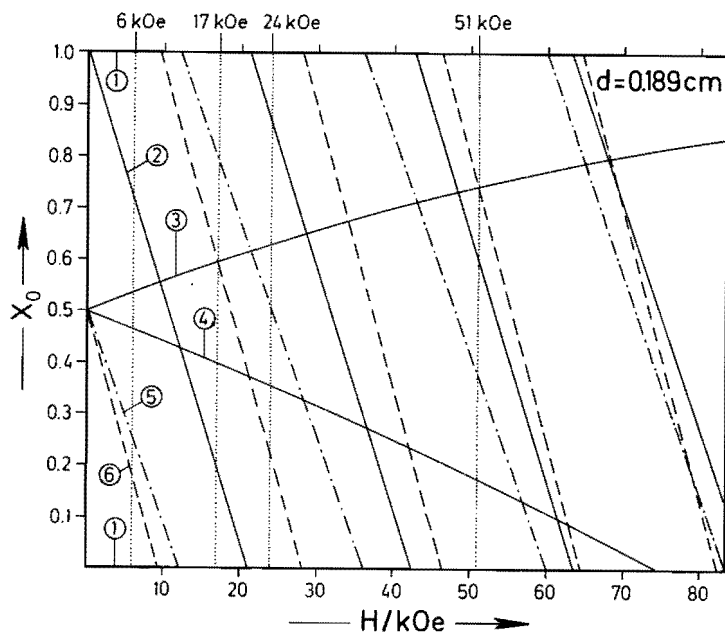


Fig. 2. Calculated pattern showing the overlap of the interference orders of the six circularly polarized Zeeman components (Na $3p^2P$ states) as a function of the magnetic field strength. The mirror distance of the Fabry-Pérot interferometer is set at 0.189 cm. Each component (No. (1) to (6)) gives, as a function of the magnetic field the relative position x_0 of the respective component. x_0 is referred, firstly, to the position of the component No. (1) and secondly, to the free spectral range of the interferometer. The numbers (1) to (6) correspond to the following Zeeman states: (1): $^2P_{1/2, -1/2}$, (2): $^2P_{1/2, +1/2}$, (3): $^2P_{3/2, -1/2}$, (4): $^2P_{3/2, -3/2}$, (5): $^2P_{3/2, +3/2}$, (6): $^2P_{3/2, +1/2}$. Measurements were performed at 6, 17, 24 and 51 kOe as indicated by vertical lines

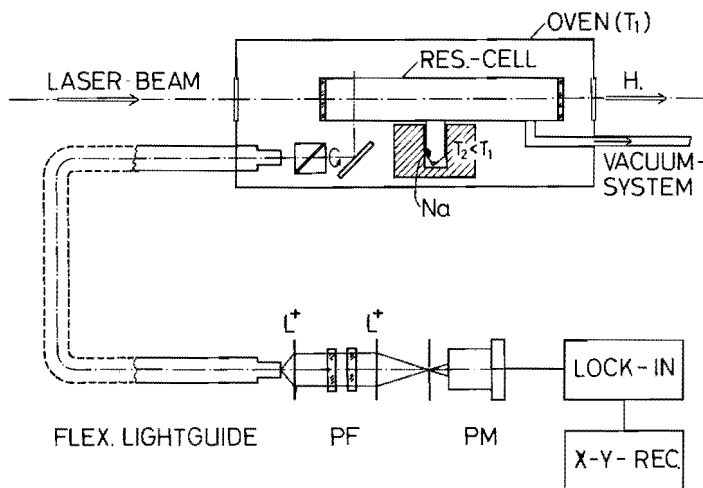


Fig. 3. Arrangement of the apparatus, *PM* photomultiplier, *PF* Pérot-Fabry interferometer, *L* lens, $T_2 = 380$ K and $T_1 = 450$ K. At $T_2 = 380$ K the optical depth of the vapor (≈ 18 cm) was a multiple of the cell dimensions. Therefore radiation trapping effects are negligible. The reference signal for the Lock-in amplifier was generated by laser beam chopping. Prior to any experiment it was ensured that scattered pumping light did not reach the detection system. By detuning the laser to some frequency far off the resonant frequencies we found out that the scattered pumping light did not exceed 1 part in 1,000 parts of fluorescent light

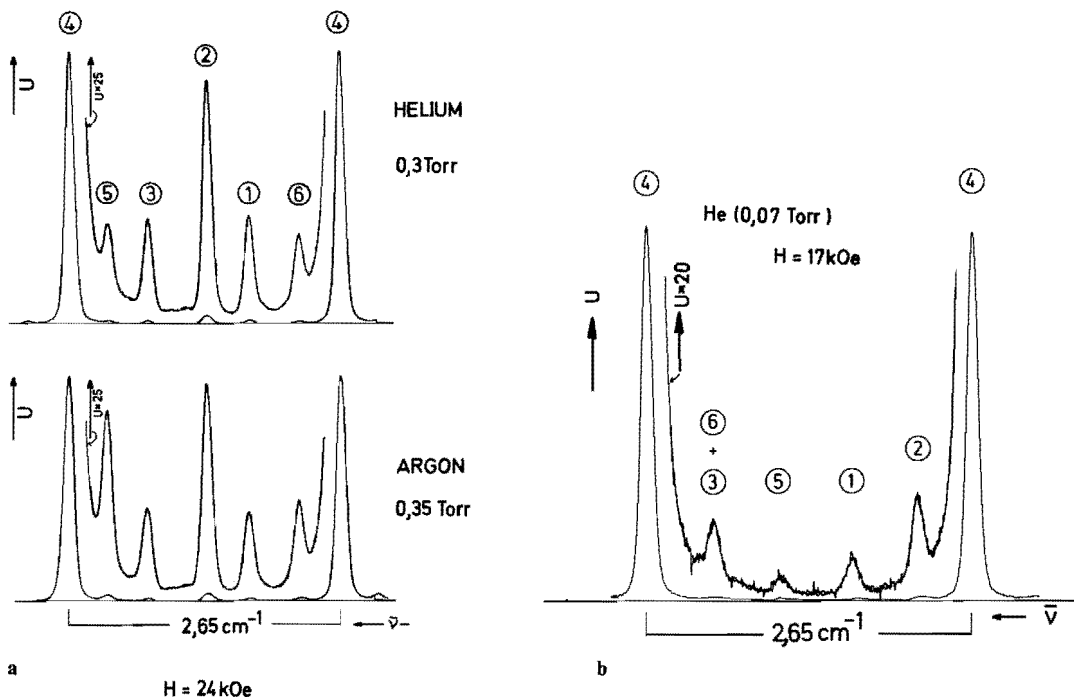


Fig. 4. a Two examples of recordings of the six fluorescence components in the case of $H = 24$ kOe, $^2P_{3/2, -3/2}$ excitation, He at 0.3 Torr, and Ar at 0.35 Torr. Each curve represents the superposition of two successive interferometer scans. The "sensitized" components (5), (3), (2), (1), (6) (notation as on Fig. 2) are registered at a 25 times greater sensitivity than the direct component (4). Naturally the evaluated measurements were taken at lower pressure (0.02 to 0.15 Torr) with a consequent reduction of the signal-to-noise ratio. Even then it was satisfactory as to be seen on Figure 4 b

b Example of a recording of the fluorescence components in the case of $H = 17$ kOe, $^2P_{3/2, -3/2}$ excitation and He at 0.07 Torr. This recording is typical for the obtained signal-to-noise ratio for the lower pressure values. The "sensitized" components (6 + 3), (5), (1), (2) (notation as on Fig. 2) are registered at a 20 times greater sensitivity than the direct component

transition probability. In particular the absence of optical pumping warrants a powerful excitation and an accumulation of large numbers of atoms in these states.

For each inert gas pressure we recorded two successive sweeps of the interferometer and changed the

sensitivity by 10 to 25 times while scanning the sensitized components. Figure 4 shows an example of two experimental curves one for He (0.3 Torr) and one for Ar (0.35 Torr). The curves were obtained for $^2P_{3/2, -3/2}$ excitation at 24 kOe. The sweep time was set at 100 s and the integration time at 0.1 s. The half width

($\approx 0.11 \text{ cm}^{-1}$) of one component in Figure 3 is determined by the half width of the Zeeman components ($\approx 0.095 \text{ cm}^{-1}$) and the "finesse" ($F=40$) of the interferometer. Laser power fluctuations during one sweep were less than 3%.

Figure 4 already shows an interesting detail, namely, the appearance of the ${}^2P_{3/2, +3/2}$ component (no. (5) in Fig. 4) due to the collision induced transition ${}^2P_{3/2, -3/2} \rightarrow {}^2P_{3/2, +3/2}$. This transition is rendered possible by a simultaneous flip of the spin and the orbital angular momentum, which is brought about by competing spin-orbit interaction during the collision process [16, 17, 19, 33]. Proceeding to Argon from the lighter rare gases we measured an enormous increase of this component which makes it the most prominent for Krypton and Xenon.

3. Theoretical

3.1. Evaluation of the Signals

The stationary solution of the rate equation for the population n_i of the i -th Zeeman state which is only excited through collisions is:

$$\frac{dn_i}{dt} = 0 = -n_i(1/\tau + \sum_{i \neq j} N v_r \sigma_{i \rightarrow j}) + \sum_{j \neq i} N v_r \sigma_{j \rightarrow i} n_j. \quad (1)$$

τ represents the lifetime of the $3p^2P$ -Zeeman states, N the density of the inert gas atoms, v_r the average relative velocity of the colliding partners and $\sigma_{i \rightarrow j}$ the cross section for the population transfer from the i -th to the j -th Zeeman state. N is connected to the inert gas pressure p as follows:

$$N = p/kT. \quad (2)$$

k represents the Boltzmann factor and T the temperature of the cell walls. The time T_c between two collisions is given by:

$$1/T_{c(i \rightarrow j)} = N v_r \sigma_{i \rightarrow j}. \quad (3)$$

The experiments were performed for inert gas pressures lower than 0.25 Torr. With (3) and the values for $\sigma_{i \rightarrow j}$ in Table 1 follows $T_{c(i \rightarrow j)} \gg \tau$ for all collision induced transitions in question. Therefore, the probability that multiple collisions happen during the lifetime τ of the Zeeman states is much reduced. As a consequence all transfer rates in (1) are negligible except those leading from the optically excited state n_k to the observed state n_i . From (1) and (2) one obtains the ratio:

$$n_i/n_k = \tau p v_r \sigma_{k \rightarrow i}/kT \quad (4)$$

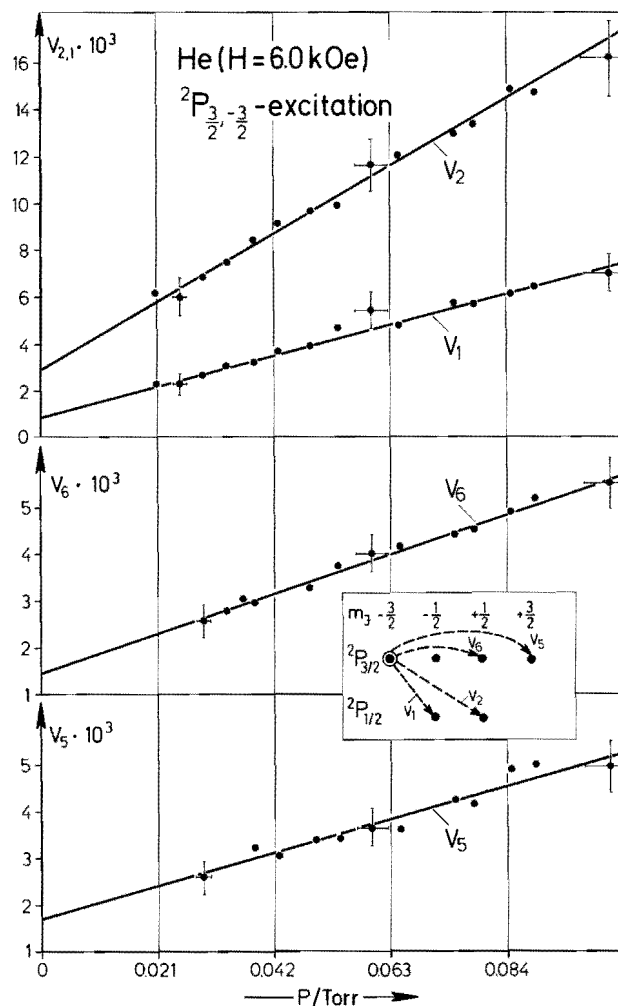


Fig. 5. Ratio of the sensitized and direct fluorescence intensities V for the indicated transitions vs. the He pressure at 6 kOe and for ${}^2P_{3/2, -3/2}$ excitation

which is connected to the sensitized and direct fluorescence intensities, I_s and I_d , in the following way:

$$\begin{aligned} V = I_s/I_d &= a_s(H)n_i/(a_d(H)n_k) \\ &= (a_s(H)/a_d(H))p v_r \tau \sigma_{k \rightarrow i}/kT; \end{aligned} \quad (5)$$

$a_s(H)$ and $a_d(H)$ represents the respective optical transition probabilities which depend on the magnetic field strength [10]. A plot of V against the inert gas pressure therefore gives straight lines and from the slope one derives by (5) the cross section $\sigma_{k \rightarrow i}$. Figure 5 shows an example of this plot for Helium at 6 kOe and ${}^2P_{3/2, -3/2}$ excitation. The collision induced transitions are indicated on the insert figure which serves to clarify the symbols V_1 , V_2 , V_5 , and V_6 . As predicted, we obtained straight lines. For $p=0$ the ratio V does not tend towards zero in contradiction to (5). This finite V value is caused by the far wing of the main line

due to the imperfect interferometer function which thus effects a parallel displacement of the straight lines.

The straight lines are fitted to the experimental points by a computer programme [11] which takes into account the errors of V (2% to 15%, depending on the experimental conditions) and the pressure errors (5%).

3.2. Remarks on the Magnetic Field Dependence of Cross Sections for the Population Transfer between Single 2P -Zeeman States

Measurements of the magnetic field dependence of cross sections for the population transfer between single Zeeman states are of interest because they offer a very simple method for varying the energy difference ΔE between two Zeeman states over a considerable range. This enables one to study collision processes in the regime where neither the condition for sudden collisions:

$$\Delta E \tau_c \ll \hbar \quad (7a)$$

nor the condition for adiabatic collisions:

$$\Delta E \tau_c \gg \hbar \quad (7b)$$

holds perfectly. (τ_c = mean duration of the collisions with $\tau_c = \sqrt{\sigma/\pi} v^{-1}$; σ = cross section for the respective transition). Respective theoretical [12] and experimental [13, 14] investigations of the collision processes where $\Delta E \tau_c \gtrsim \hbar$ have recently been reported for resonant $\text{Hg}^* - \text{Hg}$ and nonresonant $\text{Hg}^* - \text{inert gas}$ collisions [41].

In the case of nonresonant $\text{Na}^* - \text{inert gas}$ collisions the influence of the magnetic field proceeds in a two-fold way: Firstly, it changes the energy splitting and thus may shift the character of the collision from sudden to adiabatic or inverse. As a consequence, the transition probability changes drastically. Secondly, it causes a magnetic mixing of the $^2P_{3/2, \pm 1/2}$ and $^2P_{1/2, \pm 1/2}$ states which again may affect the transition probability.

The effect of energy splitting will become important for a "critical" field H_c [13] for which $\Delta E \tau_c \approx \hbar$ is valid.

In the $3p\ ^2P$ state of sodium the $^2P_{3/2, 3/2} \rightarrow ^2P_{3/2, -3/2}$ transition is particularly suited to study this effect. For this transition, on the one hand, the Zeeman splitting ΔE is the largest for all transitions in the two 2P states (see Fig. 1) and, on the other hand, the $^2P_{3/2, \pm 3/2}$ wave functions are not subject to magnetic mixing. $\Delta E \tau_c \approx \hbar$ with the respective cross sections in Table 1 yields for He a critical field of about 150 kOe and for Kr and Xe of about 50 kOe. Therefore, it should be possible to observe the influence of the energy splitting on the cross sections in the case of the heavier inert gases for H not larger than 50 kOe.

To give an idea of the magnetic state mixing effect we calculated approximately the dependence of the respective cross sections on the magnetic field strength. The calculation is straight-forward and we only give the results.

From a first order perturbation calculation one gets for the $3p\ ^2P$ wave functions:

$$\begin{aligned} |3/2, \pm 3/2\rangle(H) &= |3/2, \pm 3/2\rangle(H=0) \\ |3/2, \pm 1/2\rangle(H) &= |3/2, \pm 1/2\rangle(H=0) \\ &\quad - b(H) |1/2, \pm 1/2\rangle(H=0) \\ |1/2, \pm 1/2\rangle(H) &= |1/2, \pm 1/2\rangle(H=0) \\ &\quad + b(H) |3/2, \pm 1/2\rangle(H=0) \end{aligned} \quad (8)$$

with $b(H) = \mu_B H \sqrt{2}/3 \varepsilon = 1.28 \cdot 10^{-6} H/\text{Oe}$. ($\varepsilon \approx 17.2 \text{ cm}^{-1}$, energy difference between the $3p$ fine structure states).

To estimate cross sections for the collision induced inter Zeeman transitions we used the approximation that spin and orbital angular momentum are decoupled during the collision time τ_c . In this case the respective transition operator T [15] operates on orbital states and leaves the spin states unchanged. Similar to the calculation in [16] with the wave functions in (8) one gets respective transition probabilities and the following cross sections (terms quadratic in b have been neglected; the cross sections are given in the notation $\sigma(j, m_j \rightarrow j', m'_j)(H) = f(H) \cdot \sigma(l, m_l \rightarrow l', m'_l)$):

$$\begin{aligned} \sigma(3/2, +3/2 \rightarrow 1/2, -1/2)(H) &= (2/3 - a(H)) \sigma(1, +1 \rightarrow 1, -1)(H=0) \\ \sigma(3/2, +3/2 \rightarrow 1/2, +1/2)(H) &= (1/3 - a(H)) \sigma(1, +1 \rightarrow 1, 0)(H=0) \\ \sigma(3/2, -3/2 \rightarrow 1/2, -1/2)(H) &= (1/3 + a(H)) \sigma(1, -1 \rightarrow 1, 0)(H=0) \\ \sigma(3/2, -3/2 \rightarrow 1/2, +1/2)(H) &= (2/3 + a(H)) \sigma(1, -1 \rightarrow 1, +1)(H=0) \\ \sigma(3/2, +3/2 \rightarrow 3/2, +1/2)(H) &= (2/3 + a(H)) \sigma(1, +1 \rightarrow 1, 0)(H=0) \\ \sigma(3/2, +3/2 \rightarrow 3/2, -1/2)(H) &= (1/3 + a(H)) \sigma(1, +1 \rightarrow 1, -1)(H=0) \\ \sigma(3/2, -3/2 \rightarrow 3/2, +1/2)(H) &= (1/3 - a(H)) \sigma(1, -1 \rightarrow 1, +1)(H=0) \\ \sigma(3/2, -3/2 \rightarrow 3/2, -1/2)(H) &= (2/3 - a(H)) \sigma(1, -1 \rightarrow 1, 0)(H=0) \end{aligned}$$

with

$$a = b 2\sqrt{2}/3 = 1.21 \cdot 10^{-6} H/\text{Oe}. \quad (9)$$

This calculation shows another influence of the magnetic field. The symmetry relation $\sigma(j, m_j \rightarrow j', m'_j) = \sigma(j, -m_j \rightarrow j', -m'_j)$ which is a result of the invariance properties of the transition operator under time reversal and spatial rotation [17-19] doesn't hold any longer in the presence of a magnetic field. This is a particular illustration of a more general property given in Reference [13]. Here, only the average:

$$\bar{\sigma}(j, \pm m_j \rightarrow j', \pm m'_j) = (\sigma(j, m_j \rightarrow j', m'_j) + \sigma(j, -m_j \rightarrow j', -m'_j))/2 \quad (10)$$

is conserved to first order approximation.

To get an idea of the importance of the magnetic mixing effect we calculated values for the relative change:

$$\Delta\sigma/\sigma = (\sigma(H) - \sigma(H=0))/\sigma(H=0) \quad (11)$$

for the following transitions:

$$\begin{aligned} \Delta\sigma/\sigma(3/2, \pm 3/2 \rightarrow 1/2, \mp 1/2)(H) &= \mp 1.81 \cdot 10^{-6} H/\text{Oe} \\ \Delta\sigma/\sigma(3/2, \pm 3/2 \rightarrow 1/2, \pm 1/2)(H) &= \mp 3.62 \cdot 10^{-6} H/\text{Oe}. \end{aligned} \quad (12)$$

For 50 kOe one obtains a relative change of about 10% and 20%, respectively with this model.

4. Experimental Results and Discussion

In Tables 1 and 2 the measured cross sections together with their absolute errors are listed. The relative errors vary in the range of 5% to 20%, approximately, depending on the respective experimental conditions (e. g. stability of the laser, choice of the initially excited state, position in the spectrum and intensity of the measured fluorescence components). The magnetic field dependence was only measured for the favourable ${}^2P_{3/2, \pm 3/2}$ excitation. Similar measurements for ${}^2P_{1/2, \pm 1/2}$ excitation are in progress.

In the following the experimental data in Tables 1 and 2 are discussed under various aspects:

4.1. Magnetic Field Dependence

Table 1 shows that for magnetic field strengths of less than 24 kOe the cross sections conform to the symmetry relation $\sigma(j, +m_j \rightarrow j', +m'_j) = \sigma(j, -m_j \rightarrow j', -m'_j)$ within the experimental error limit. For higher fields systematic deviations become apparent. The influence is less important for the ${}^2P_{3/2, \pm 3/2} \rightarrow {}^2P_{1/2, \pm 1/2}$ transitions but rather drastic for the ${}^2P_{3/2, \pm 3/2} \rightarrow {}^2P_{1/2, \mp 1/2}$ transition and significant above the error limit.

In Table 3 we calculated the relative change $\Delta\sigma/\sigma$ for the measured cross sections according to (11) for 51 kOe and the five inert gases. In addition the ex-

pected $\Delta\sigma/\sigma$ values at 51 kOe and the energy change ΔE between the respective Zeeman states are given.

One concludes from Table 3 the following trends:

a) The sign of $\Delta\sigma/\sigma$ agrees in all cases with the calculated one.

b) $\Delta\sigma/\sigma(3/2, \pm 3/2 \rightarrow 1/2, \mp 1/2)$ agrees for He and Ne with the calculation. For Ar, Kr, and Xe one observes an increase for $\Delta\sigma/\sigma$ with the tendency:

$$\begin{aligned} &|\Delta\sigma/\sigma(3/2, +3/2 \rightarrow 1/2, -1/2)| \\ &< |\Delta\sigma/\sigma(3/2, -3/2 \rightarrow 1/2, +1/2)|. \end{aligned}$$

c) $\Delta\sigma/\sigma(3/2, \pm 3/2 \rightarrow 1/2, \pm 1/2)$ agrees with the calculated values within the experimental error limit.

The behaviour mentioned in b) may be explained by an additional energy effect which is expected for the heavier inert gases and by the imperfect approximation in Section 3.2. The transition operator T applied in 3.2 is only valid if a complete decoupling of spin and orbital momentum during the collision time is assured. This assumption is no longer valid for heavier inert gases as there the expectation value of the total angular momentum becomes more and more a good quantum number during the collision process.

From the last column in Table 3 it follows that the decrease of $\sigma(3/2, +3/2 \rightarrow 1/2, -1/2)$ and the increase of $\sigma(3/2, -3/2 \rightarrow 1/2, +1/2)$ proceed in accordance with the increase or decrease of the energy difference between the respective states. For these transitions the energy and the magnetic mixing effect tend in the same direction and reinforce each other.

Obviously, $\sigma(3/2, -3/2 \rightarrow 1/2, +1/2)$ is more affected than $\sigma(3/2, +3/2 \rightarrow 1/2, -1/2)$ and it would be rather interesting to study this effect for higher magnetic fields up to the crossing point of the ${}^2P_{3/2, -3/2}$ and ${}^2P_{1/2, +1/2}$ state as we plan to do. In Table 4 we calculated the average values $\bar{\sigma}(j, \pm m_j \rightarrow j', \pm m'_j)$ for the indicated transitions and the five inert gases. These values serve to prove whether magnetic mixing effects influence symmetrically respective cross sections as predicted in Section 3.2. As can be seen in Table 4 this prediction is confirmed in all cases except for $\bar{\sigma}(3/2, \pm 3/2 \rightarrow 1/2, \mp 1/2)$ obtained at 51 kOe for Ar, Kr and Xe.

The expected energy effect on $\bar{\sigma}(3/2, \pm 3/2 \rightarrow 3/2, \mp 3/2)$ is only to be seen in its trend for Kr and Xe. The diminution of this cross sections at high magnetic fields is still obscured by the experimental errors.

4.2. Multipole Transfer ($k=0, 1$) and Relaxation ($k=1, 2, 3$) Cross Sections and the Comparison with other Experiments

In Section 4.1 we proved that magnetic mixing effects for $H \leq 24$ kOe cancel when taking the average cross sections according to (10). Furthermore, energetic

Table 1a-c. Measured cross sections $\sigma(j, m_j \rightarrow j', m'_j)$ obtained for Na $3p^2P_{3/2, \pm 3/2}$ excitation and various magnetic field strengths for the five inert gases. The values in brackets are obtained from those at 24 kOe with [10]**Table 1a**

σ	H							
	6 kOe	17 kOe	24 kOe	51 kOe	6 kOe	17 kOe	24 kOe	51 kOe
	Helium ($T=450$ K)				Neon ($T=450$ K)			
$\sigma(\frac{3}{2}, \frac{3}{2} \rightarrow \frac{1}{2}, -\frac{1}{2})/\text{\AA}^2$	34.9 ± 3.1	35.6 ± 3.0	32.0 ± 2.8	29.5 ± 3.5	25.9 ± 2.4	25.0 ± 2.3	22.3 ± 2.1	22.6 ± 2.1
$\sigma(\frac{3}{2}, \frac{3}{2} \rightarrow \frac{1}{2}, +\frac{1}{2})/\text{\AA}^2$	15.4 ± 1.7	15.1 ± 1.7	13.9 ± 1.4	12.6 ± 2.5	12.1 ± 1.5	12.6 ± 1.4	11.9 ± 1.4	10.1 ± 1.5
$\sigma(\frac{3}{2}, \frac{3}{2} \rightarrow \frac{3}{2}, -\frac{1}{2})/\text{\AA}^2$	23.2 ± 3.5	—	23.9 ± 3.5	—	23.0 ± 3.4	—	24.5 ± 3.2	—
$\sigma(\frac{3}{2}, \frac{3}{2} \rightarrow \frac{3}{2}, -\frac{3}{2})/\text{\AA}^2$	5.4 ± 0.8	5.3 ± 0.8	5.3 ± 1.0	5.2 ± 1.0	9.5 ± 1.2	8.9 ± 1.0	8.1 ± 1.2	8.2 ± 1.0
$\sigma(\frac{3}{2}, \frac{3}{2} \rightarrow \frac{3}{2}, +\frac{1}{2})/\text{\AA}^2$	(28.3 ± 2.5)	—	29.9 ± 3.5	—	(24.1 ± 2.5)	—	24.6 ± 3.5	—
$\sigma(\frac{3}{2}, -\frac{3}{2} \rightarrow \frac{1}{2}, -\frac{1}{2})/\text{\AA}^2$	16.1 ± 2.0	16.5 ± 1.7	16.9 ± 1.9	18.3 ± 2.8	14.1 ± 1.7	14.8 ± 1.8	14.2 ± 2.0	17.2 ± 1.9
$\sigma(\frac{3}{2}, -\frac{3}{2} \rightarrow \frac{1}{2}, +\frac{1}{2})/\text{\AA}^2$	35.9 ± 3.5	34.7 ± 3.2	37.1 ± 3.6	40.1 ± 4.2	27.5 ± 3.0	26.7 ± 2.5	26.3 ± 2.7	31.3 ± 2.9
$\sigma(\frac{3}{2}, -\frac{3}{2} \rightarrow \frac{3}{2}, -\frac{1}{2})/\text{\AA}^2$	(28.3 ± 2.5)	—	26.6 ± 3.5	—	(24.1 ± 2.5)	—	23.5 ± 3.6	—
$\sigma(\frac{3}{2}, -\frac{3}{2} \rightarrow \frac{3}{2}, +\frac{3}{2})/\text{\AA}^2$	5.7 ± 0.9	5.5 ± 0.8	5.2 ± 1.0	4.8 ± 1.0	9.4 ± 1.2	8.8 ± 1.1	8.0 ± 1.2	8.1 ± 0.9
$\sigma(\frac{3}{2}, -\frac{3}{2} \rightarrow \frac{3}{2}, +\frac{1}{2})/\text{\AA}^2$	22.9 ± 3.5	—	18.8 ± 3.5	—	22.7 ± 3.1	—	17.8 ± 4.0	—

Table 1b

σ	Argon ($T=450$ K)				Krypton ($T=450$ K)			
	6 kOe	17 kOe	24 kOe	51 kOe	6 kOe	17 kOe	24 kOe	51 kOe
$\sigma(\frac{3}{2}, \frac{3}{2} \rightarrow \frac{1}{2}, -\frac{1}{2})/\text{\AA}^2$	43.8 ± 4.0	41.6 ± 3.5	41.1 ± 3.9	38.4 ± 3.7	35.4 ± 3.0	34.3 ± 2.7	32.7 ± 2.7	28.9 ± 2.2
$\sigma(\frac{3}{2}, \frac{3}{2} \rightarrow \frac{1}{2}, +\frac{1}{2})/\text{\AA}^2$	19.3 ± 2.3	18.9 ± 2.0	17.2 ± 2.0	15.2 ± 2.0	17.5 ± 1.7	17.3 ± 1.6	16.8 ± 1.6	16.0 ± 1.6
$\sigma(\frac{3}{2}, \frac{3}{2} \rightarrow \frac{3}{2}, -\frac{1}{2})/\text{\AA}^2$	45.2 ± 6.0	—	48.4 ± 5.5	—	58.5 ± 7.0	—	59.6 ± 5.8	—
$\sigma(\frac{3}{2}, \frac{3}{2} \rightarrow \frac{3}{2}, -\frac{3}{2})/\text{\AA}^2$	25.8 ± 2.4	25.0 ± 2.3	23.9 ± 2.2	23.0 ± 2.2	42.3 ± 3.5	40.6 ± 3.2	39.6 ± 3.2	36.7 ± 2.9
$\sigma(\frac{3}{2}, \frac{3}{2} \rightarrow \frac{3}{2}, +\frac{1}{2})/\text{\AA}^2$	(39.5 ± 4.1)	—	42.5 ± 5.6	—	(57.7 ± 4.4)	—	60.2 ± 6.5	—
$\sigma(\frac{3}{2}, -\frac{3}{2} \rightarrow \frac{1}{2}, -\frac{1}{2})/\text{\AA}^2$	18.5 ± 2.4	19.4 ± 2.6	21.5 ± 3.4	23.9 ± 3.2	19.4 ± 2.0	21.6 ± 1.8	20.9 ± 1.8	24.4 ± 2.0
$\sigma(\frac{3}{2}, -\frac{3}{2} \rightarrow \frac{1}{2}, +\frac{1}{2})/\text{\AA}^2$	43.4 ± 4.1	48.5 ± 5.0	48.2 ± 5.3	56.5 ± 6.0	39.8 ± 3.5	42.7 ± 3.6	44.1 ± 3.6	52.8 ± 4.5
$\sigma(\frac{3}{2}, -\frac{3}{2} \rightarrow \frac{3}{2}, -\frac{1}{2})/\text{\AA}^2$	(39.5 ± 4.1)	—	36.5 ± 4.5	—	(57.7 ± 4.4)	—	55.2 ± 5.8	—
$\sigma(\frac{3}{2}, -\frac{3}{2} \rightarrow \frac{3}{2}, +\frac{3}{2})/\text{\AA}^2$	25.8 ± 2.5	25.1 ± 2.2	24.1 ± 3.0	25.0 ± 3.0	42.9 ± 3.7	41.0 ± 3.3	39.6 ± 3.1	35.4 ± 2.8
$\sigma(\frac{3}{2}, -\frac{3}{2} \rightarrow \frac{3}{2}, +\frac{1}{2})/\text{\AA}^2$	41.0 ± 6.0	—	35.6 ± 5.5	—	59.6 ± 6.9	—	50.7 ± 6.0	—

Table 1c

σ	Xenon ($T=450$ K)			
	6 kOe	17 kOe	24 kOe	51 kOe
$\sigma(\frac{3}{2}, \frac{3}{2} \rightarrow \frac{1}{2}, -\frac{1}{2})/\text{\AA}^2$	32.9 ± 2.8	34.0 ± 3.2	30.8 ± 2.7	25.9 ± 4.1
$\sigma(\frac{3}{2}, \frac{3}{2} \rightarrow \frac{1}{2}, +\frac{1}{2})/\text{\AA}^2$	18.1 ± 1.7	18.5 ± 2.3	18.6 ± 1.9	15.8 ± 1.8
$\sigma(\frac{3}{2}, \frac{3}{2} \rightarrow \frac{3}{2}, -\frac{1}{2})/\text{\AA}^2$	62.8 ± 7.0	—	70.0 ± 7.5	—
$\sigma(\frac{3}{2}, \frac{3}{2} \rightarrow \frac{3}{2}, -\frac{3}{2})/\text{\AA}^2$	45.1 ± 3.8	46.2 ± 3.9	45.1 ± 3.7	40.3 ± 3.4
$\sigma(\frac{3}{2}, \frac{3}{2} \rightarrow \frac{3}{2}, +\frac{1}{2})/\text{\AA}^2$	(64.7 ± 5.1)	—	70.2 ± 6.8	—
$\sigma(\frac{3}{2}, -\frac{3}{2} \rightarrow \frac{1}{2}, -\frac{1}{2})/\text{\AA}^2$	19.1 ± 1.7	21.0 ± 2.0	21.9 ± 3.7	24.0 ± 3.2
$\sigma(\frac{3}{2}, -\frac{3}{2} \rightarrow \frac{1}{2}, +\frac{1}{2})/\text{\AA}^2$	35.4 ± 2.9	37.7 ± 3.4	44.4 ± 4.8	52.6 ± 4.7
$\sigma(\frac{3}{2}, -\frac{3}{2} \rightarrow \frac{3}{2}, -\frac{1}{2})/\text{\AA}^2$	(64.7 ± 5.1)	—	59.1 ± 7.5	—
$\sigma(\frac{3}{2}, -\frac{3}{2} \rightarrow \frac{3}{2}, +\frac{3}{2})/\text{\AA}^2$	46.1 ± 3.8	45.4 ± 3.7	44.4 ± 4.2	40.6 ± 3.6
$\sigma(\frac{3}{2}, -\frac{3}{2} \rightarrow \frac{3}{2}, +\frac{1}{2})/\text{\AA}^2$	62.6 ± 6.9	—	55.5 ± 6.5	—

effects are negligible in this field range and from 6 kOe upward the cross sections are no longer influenced by nuclear spin effects [7, 21–23] as nuclear spin and orbital momentum are perfectly decoupled. Thus, these experimental values are rather suited for a comparison with respective experimental and theoretical

data which have already been published. Therefore we calculated from the average values $\bar{\sigma}(j, \pm m_j \rightarrow j', \pm m'_j)$ at 6 kOe transfer and relaxation cross sections for the 2P macroscopic tensor components of the degree $k=0, 1, 2$, and 3 according to the relations and notations given in [20]. For the calculation of $\sigma_{3/2 \rightarrow 1/2}^{(1)}$

Table 2. Measured cross sections $\sigma(j, m_j \rightarrow j', m'_j)$ obtained for Na $3p\ ^2P_{1/2, \pm 1/2}$ excitation, a magnetic field strength of 6 kOe, and the five inert gases. In the last row $\sigma_{1/2 \rightarrow 3/2}^{(0)}$ represents the cross sections for the excitation transfer from the $^2P_{1/2}$ to the $^2P_{3/2}$ state which were directly measured in zero magnetic field

	He	Ne	Ar	Kr	Xe	H/kOe
$\sigma(\frac{1}{2}, -\frac{1}{2} \rightarrow \frac{1}{2}, +\frac{1}{2})/\text{\AA}^2$	13.7 ± 2.6	14.6 ± 3.3	29.2 ± 4.0	63.0 ± 5.6	71.5 ± 7.4	6
$\sigma(\frac{1}{2}, -\frac{1}{2} \rightarrow \frac{3}{2}, -\frac{1}{2})/\text{\AA}^2$	21.7 ± 5.1	21.9 ± 7.2	29.3 ± 6.8	26.3 ± 3.8	23.3 ± 7.0	6
$\sigma(\frac{1}{2}, -\frac{1}{2} \rightarrow \frac{3}{2}, -\frac{3}{2})/\text{\AA}^2$	14.9 ± 2.0	13.2 ± 2.3	20.6 ± 2.7	18.6 ± 1.8	18.4 ± 3.3	6
$\sigma(\frac{1}{2}, -\frac{1}{2} \rightarrow \frac{3}{2}, +\frac{3}{2})/\text{\AA}^2$	34.7 ± 3.4	24.8 ± 3.0	45.8 ± 4.4	34.4 ± 3.1	30.0 ± 3.8	6
$\sigma(\frac{1}{2}, -\frac{1}{2} \rightarrow \frac{3}{2}, +\frac{1}{2})/\text{\AA}^2$	31.1 ± 5.8	20.9 ± 6.0	34.2 ± 8.0	30.9 ± 3.9	25.8 ± 8.4	6
$\sigma(\frac{1}{2}, +\frac{1}{2} \rightarrow \frac{1}{2}, -\frac{1}{2})/\text{\AA}^2$	12.6 ± 2.5	13.7 ± 3.3	30.5 ± 3.5	65.5 ± 5.4	72.8 ± 8.0	6
$\sigma(\frac{1}{2}, +\frac{1}{2} \rightarrow \frac{3}{2}, -\frac{1}{2})/\text{\AA}^2$	31.8 ± 5.5	20.9 ± 6.5	35.5 ± 7.0	33.1 ± 4.3	25.9 ± 7.5	6
$\sigma(\frac{1}{2}, +\frac{1}{2} \rightarrow \frac{3}{2}, -\frac{3}{2})/\text{\AA}^2$	35.5 ± 3.5	26.7 ± 3.3	46.4 ± 4.2	40.2 ± 3.4	33.6 ± 6.1	6
$\sigma(\frac{1}{2}, +\frac{1}{2} \rightarrow \frac{3}{2}, +\frac{3}{2})/\text{\AA}^2$	15.9 ± 2.1	13.8 ± 2.4	18.4 ± 2.3	18.6 ± 1.9	16.6 ± 6.0	6
$\sigma(\frac{1}{2}, +\frac{1}{2} \rightarrow \frac{3}{2}, +\frac{1}{2})/\text{\AA}^2$	26.8 ± 5.4	20.0 ± 7.5	32.9 ± 5.4	28.9 ± 4.5	26.0 ± 8.0	6
$\sigma_{1/2 \rightarrow 3/2}^{(0)}/\text{\AA}^2$	107.3 ± 5.1	77.4 ± 3.8	128.5 ± 10.3	112.3 ± 6.5	105.5 ± 6.0	0

Table 3. Relative change $\Delta\sigma/\sigma = (\sigma(51\text{kOe}) - \sigma(6\text{kOe}))/\sigma(6\text{kOe})$ for the five inert gases compared with calculated values. $\Delta E = E(51\text{kOe}) - E(6\text{kOe})$ gives the change of the energy difference between the respective Zeeman states

	He	Ne	Ar	Kr	Xe	Eq. (12) (51 kOe)	$\frac{\Delta E}{\text{cm}^{-1}}$
$\Delta\sigma/\sigma(\frac{3}{2}, +\frac{3}{2} \rightarrow \frac{1}{2}, -\frac{1}{2})$	-0.15 ± 0.13	-0.13 ± 0.11	-0.12 ± 0.12	-0.18 ± 0.09	-0.21 ± 0.14	-0.09	+4.8
$\Delta\sigma/\sigma(\frac{3}{2}, +\frac{3}{2} \rightarrow \frac{1}{2}, +\frac{1}{2})$	-0.18 ± 0.19	-0.17 ± 0.16	-0.21 ± 0.14	-0.09 ± 0.13	-0.13 ± 0.14	-0.18	+3.5
$\Delta\sigma/\sigma(\frac{3}{2}, -\frac{3}{2} \rightarrow \frac{1}{2}, -\frac{1}{2})$	+0.14 ± 0.22	+0.22 ± 0.20	+0.29 ± 0.24	+0.26 ± 0.17	+0.26 ± 0.20	+0.18	-3.5
$\Delta\sigma/\sigma(\frac{3}{2}, -\frac{3}{2} \rightarrow \frac{1}{2}, +\frac{1}{2})$	+0.12 ± 0.16	+0.14 ± 0.16	+0.30 ± 0.19	+0.33 ± 0.16	+0.46 ± 0.18	+0.09	-4.7

Table 4. Average cross sections $\bar{\sigma}(j, \pm m_j \rightarrow j', \pm m'_j)$ for three pairs of transitions at 6, 17, 24, and 51 kOe and for the five inert gases

	6 kOe	17 kOe	24 kOe	51 kOe	
$\bar{\sigma}(\frac{3}{2}, \pm\frac{3}{2} \rightarrow \frac{1}{2}, \mp\frac{1}{2})/\text{\AA}^2$	35.4 ± 2.3	35.2 ± 2.2	34.6 ± 2.3	34.8 ± 2.7	He
$\bar{\sigma}(\frac{3}{2}, \pm\frac{3}{2} \rightarrow \frac{1}{2}, \pm\frac{1}{2})/\text{\AA}^2$	15.8 ± 1.3	15.8 ± 1.2	15.4 ± 1.2	15.5 ± 1.9	
$\bar{\sigma}(\frac{3}{2}, \pm\frac{3}{2} \rightarrow \frac{3}{2}, \mp\frac{3}{2})/\text{\AA}^2$	5.6 ± 0.6	5.4 ± 0.6	5.3 ± 0.5	5.0 ± 0.5	
$\bar{\sigma}(\frac{3}{2}, \pm\frac{3}{2} \rightarrow \frac{1}{2}, \mp\frac{1}{2})/\text{\AA}^2$	26.7 ± 1.9	25.9 ± 1.7	24.3 ± 1.7	27.0 ± 1.8	Ne
$\bar{\sigma}(\frac{3}{2}, \pm\frac{3}{2} \rightarrow \frac{1}{2}, \pm\frac{1}{2})/\text{\AA}^2$	13.1 ± 1.2	13.7 ± 1.1	13.1 ± 1.2	13.9 ± 1.2	
$\bar{\sigma}(\frac{3}{2}, \pm\frac{3}{2} \rightarrow \frac{3}{2}, \mp\frac{3}{2})/\text{\AA}^2$	9.5 ± 0.9	8.9 ± 0.8	8.1 ± 0.8	8.2 ± 0.5	
$\bar{\sigma}(\frac{3}{2}, \pm\frac{3}{2} \rightarrow \frac{1}{2}, \mp\frac{1}{2})/\text{\AA}^2$	43.6 ± 2.9	45.1 ± 3.1	44.7 ± 3.3	47.5 ± 3.5	Ar
$\bar{\sigma}(\frac{3}{2}, \pm\frac{3}{2} \rightarrow \frac{1}{2}, \pm\frac{1}{2})/\text{\AA}^2$	18.9 ± 1.7	19.2 ± 1.6	19.4 ± 2.0	19.6 ± 1.9	
$\bar{\sigma}(\frac{3}{2}, \pm\frac{3}{2} \rightarrow \frac{3}{2}, \mp\frac{3}{2})/\text{\AA}^2$	25.8 ± 1.7	25.1 ± 1.5	24.0 ± 1.9	24.0 ± 1.9	
$\bar{\sigma}(\frac{3}{2}, \pm\frac{3}{2} \rightarrow \frac{1}{2}, \mp\frac{1}{2})/\text{\AA}^2$	37.6 ± 2.3	38.5 ± 2.3	38.4 ± 2.3	40.9 ± 2.5	Kr
$\bar{\sigma}(\frac{3}{2}, \pm\frac{3}{2} \rightarrow \frac{1}{2}, \pm\frac{1}{2})/\text{\AA}^2$	18.5 ± 1.3	19.5 ± 1.2	18.9 ± 1.2	20.2 ± 1.3	
$\bar{\sigma}(\frac{3}{2}, \pm\frac{3}{2} \rightarrow \frac{3}{2}, \mp\frac{3}{2})/\text{\AA}^2$	42.6 ± 2.6	40.8 ± 2.3	39.6 ± 2.3	36.1 ± 2.0	
$\bar{\sigma}(\frac{3}{2}, \pm\frac{3}{2} \rightarrow \frac{1}{2}, \mp\frac{1}{2})/\text{\AA}^2$	34.2 ± 2.0	35.9 ± 2.3	37.6 ± 2.8	39.3 ± 3.1	Xe
$\bar{\sigma}(\frac{3}{2}, \pm\frac{3}{2} \rightarrow \frac{1}{2}, \pm\frac{1}{2})/\text{\AA}^2$	18.6 ± 1.2	19.8 ± 1.5	20.3 ± 2.1	19.9 ± 1.8	
$\bar{\sigma}(\frac{3}{2}, \pm\frac{3}{2} \rightarrow \frac{3}{2}, \mp\frac{3}{2})/\text{\AA}^2$	45.6 ± 2.7	45.8 ± 2.7	44.8 ± 2.8	40.5 ± 2.5	

we applied the equally valid relation:

$$\sigma_{3/2 \rightarrow 1/2}^{(1)} = (\sigma(3/2, \pm 3/2 \rightarrow 1/2, \pm 1/2) - \sigma(3/2, \mp 3/2 \rightarrow 1/2, \pm 1/2))/3 \quad (13)$$

which suits our experimental conditions.

The cross sections thus obtained are listed in Table 5 along with previously measured values. In Table 6 we give the cross sections for the transfer $^2P_{3/2, \pm 3/2} \rightarrow ^2P_{3/2, \mp 3/2}$ and $^2P_{1/2, \pm 1/2} \rightarrow ^2P_{1/2, \mp 1/2}$. The excitation transfer cross sections $\sigma_{1/2 \rightarrow 3/2}^{(0)}$ which were measured directly in zero magnetic field (Table 5)

Table 5. Cross sections for the transfer and the relaxation of the macroscopic 2P tensor components of degree $k \leq 3$ deduced from the population transfer cross sections $\bar{\sigma}$ at 6 kOe (Tables 4 and 6) between single 2P Zeeman states for the five inert gases. For comparison previous measurements are given. $\sigma_{1/2 \rightarrow 3/2}^{(0)}$ in the first row was directly measured at $H=0$. The negative sign of $\sigma_{j \rightarrow j'}^{(1)}$ indicates that the transferred polarization ($k=1$) has the sign opposite to the initial polarization

	He	Ne	Ar	Kr	Xe	
$\sigma_{1/2 \rightarrow 3/2}^{(0)}/\text{\AA}^2$	107.3 \pm 5.1	77.4 \pm 3.8	128.5 \pm 10.3	112.3 \pm 6.5	105.5 \pm 6.0	present work, $H=0$
$\sigma_{1/2 \rightarrow 3/2}^{(0)}/\text{\AA}^2$	106.3 \pm 6.2	81.0 \pm 7.4	131.6 \pm 9.4	115.5 \pm 4.9	99.9 \pm 9.2	present work
$\sigma_{1/2 \rightarrow 3/2}^{(0)}/\text{\AA}^2$	86.0 \pm 4.3	67.0 \pm 3.4	109.9 \pm 5.5	85.0 \pm 4.3	89.8 \pm 4.5	[24]
$\sigma_{1/2 \rightarrow 3/2}^{(0)}/\text{\AA}^2$	89 \pm 9	79 \pm 8	116 \pm 12	94 \pm 10	99 \pm 10	[7]
$\sigma_{1/2 \rightarrow 3/2}^{(0)}/\text{\AA}^2$	72.4	88.9	107.5	123.6	132.7	[39]
$\sigma_{3/2 \rightarrow 1/2}^{(0)}/\text{\AA}^2$	51.2 \pm 3.3	39.8 \pm 2.3	62.5 \pm 3.4	56.1 \pm 2.7	52.8 \pm 2.5	present work
$\sigma_{1/2 \rightarrow 3/2}^{(1)}/\text{\AA}^2$	-66.3 \pm 10.3	-36.8 \pm 11.0	-83.6 \pm 13.0	-60.5 \pm 8.9	-44.1 \pm 16.7	present work
$\sigma_{1/2 \rightarrow 3/2}^{(1)}/\text{\AA}^2$	-67.8 \pm 7.0	-54.9 \pm 6.0	-87.6 \pm 9.0	-58.9 \pm 6.0	-45.7 \pm 5.0	[7]
$\sigma_{3/2 \rightarrow 1/2}^{(1)}/\text{\AA}^2$	-6.5 \pm 1.1	-4.5 \pm 0.8	-8.2 \pm 1.1	-6.4 \pm 0.9	-5.2 \pm 0.8	present work
$\sigma_{3/2 \rightarrow 1/2}^{(1)}/\text{\AA}^2$	-7.1 \pm 0.7	-5.7 \pm 0.6	-9.3 \pm 0.9	-6.2 \pm 0.6	-4.9 \pm 0.5	[7]
$\sigma_{3/2}^{(1)}/\text{\AA}^2$	112 \pm 6	105 \pm 5	198 \pm 8	259 \pm 10	271 \pm 10	present work
$\sigma_{3/2}^{(2)}/\text{\AA}^2$	154 \pm 8	134 \pm 8	228 \pm 13	290 \pm 15	308 \pm 15	present work
$\sigma_{3/2}^{(3)}/\text{\AA}^2$	129 \pm 12	109 \pm 12	186 \pm 17	254 \pm 22	277 \pm 24	present work
$\sigma_{3/2}^{(2)}/\sigma_{3/2}^{(1)}$	1.38 \pm 0.10	1.28 \pm 0.10	1.15 \pm 0.08	1.12 \pm 0.07	1.14 \pm 0.07	present work
$\sigma_{3/2}^{(3)}/\sigma_{3/2}^{(1)}$	1.15 \pm 0.12	1.04 \pm 0.12	0.94 \pm 0.09	0.98 \pm 0.09	1.02 \pm 0.10	present work
$\sigma_{1/2}^{(1)}/\text{\AA}^2$	133 \pm 7	110 \pm 9	191 \pm 10	244 \pm 9	244 \pm 12	present work
$\sigma_{1/2}^{(1)}/\text{\AA}^2$	146 \pm 22	137 \pm 21	260 \pm 39	306 \pm 46	356 \pm 53	[22]
$\sigma_{3/2}^{(1)}/\text{\AA}^2$	128 \pm 13	107 \pm 11	205 \pm 21	243 \pm 25	281 \pm 28	[21]
$\sigma_{3/2}^{(2)}/\text{\AA}^2$	167 \pm 17	174 \pm 18	308 \pm 31	341 \pm 34	376 \pm 38	[20]

Table 6. Cross sections $\bar{\sigma}$ at 6 kOe for the transitions ${}^2P_{3/2, +3/2} \rightarrow {}^2P_{3/2, -3/2}$ and ${}^2P_{1/2, +1/2} \rightarrow {}^2P_{1/2, -1/2}$ and comparison with other values in the literature. $\sigma(3/2, \pm 1/2 \rightarrow 3/2, \mp 1/2)$ is calculated from the Grawert parameters in Table 8

	He	Ne	Ar	Kr	Xe	
$\bar{\sigma}(\frac{1}{2}, \pm \frac{1}{2} \rightarrow \frac{1}{2}, \mp \frac{1}{2})/\text{\AA}^2$	13.2 \pm 1.8	14.2 \pm 2.3	29.9 \pm 2.7	64.3 \pm 3.9	72.2 \pm 5.4	present work
$\bar{\sigma}(\frac{1}{2}, \pm \frac{1}{2} \rightarrow \frac{1}{2}, \mp \frac{1}{2})/\text{\AA}^2$	16.7 \pm 1.7	16.7 \pm 1.7	32.8 \pm 3.3	69.3 \pm 6.9	91.4 \pm 9.1	[7]
$\bar{\sigma}(\frac{1}{2}, \pm \frac{1}{2} \rightarrow \frac{1}{2}, \mp \frac{1}{2})/\text{\AA}^2$	14.1 \pm 2.0	13.9 \pm 2.0	28.5 \pm 4.0	39.0 \pm 5.0	43.5 \pm 6.5	[31] ^a
$\bar{\sigma}(\frac{3}{2}, \pm \frac{3}{2} \rightarrow \frac{3}{2}, \mp \frac{3}{2})/\text{\AA}^2$	5.6 \pm 0.6	9.5 \pm 0.8	25.8 \pm 1.8	42.6 \pm 2.6	45.6 \pm 2.7	present work
$\bar{\sigma}(\frac{3}{2}, \pm \frac{3}{2} \rightarrow \frac{3}{2}, \mp \frac{1}{2})/\text{\AA}^2$	23.1 \pm 2.5	22.9 \pm 2.4	43.1 \pm 4.3	59.1 \pm 5.0	62.7 \pm 5.1	present work
$\bar{\sigma}(\frac{3}{2}, \pm \frac{3}{2} \rightarrow \frac{3}{2}, \pm \frac{1}{2})/\text{\AA}^2$	28.3 \pm 2.5	24.1 \pm 2.5	39.5 \pm 4.1	57.7 \pm 4.5	64.7 \pm 5.1	present work
$\bar{\sigma}(\frac{3}{2}, \pm \frac{1}{2} \rightarrow \frac{3}{2}, \mp \frac{1}{2})/\text{\AA}^2$	14 \pm 5	9 \pm 5	28 \pm 6	52 \pm 10	60 \pm 10	present work

^a These values were derived from the original values in [31] by dividing by two according to the definition of $\sigma_{1/2}^{(0)} = 2\sigma(1/2, \pm 1/2 \rightarrow 1/2, \mp 1/2)$ used in [31]

agree well with the derived cross sections in line 2 and 6 of Table 5. Within the experimental error $\sigma_{3/2 \rightarrow 1/2}^{(0)}$ is about twice as small as $\sigma_{1/2 \rightarrow 3/2}^{(0)}$ as expected from the principle of detailed balancing. The cross sections $\sigma_{j \rightarrow j'}^{(0)}$ of the present investigation are larger than values already published [7, 24].

Much theoretical work has already been devoted to the fine structure transitions and the respective cross sections $\sigma_{j \rightarrow j'}^{(0)}$ and $\sigma_{j \rightarrow j'}^{(1)}$. The molecular model for fine structure transitions and its application to Na-inert gas collisions is given by Nikitin, Dashevskaja et al. [4, 25–28] and Masnou and McCarroll [29, 30]. In accordance with this model the increase of $\sigma_{1/2 \rightarrow 3/2}^{(0)}$ from Ne to Ar is due to the increase of the critical

radius R_{crit} signified by:

$$\Delta V(R_{\text{crit}}) \approx \varepsilon \quad (14)$$

(notations as in [30]).

However, when the atomic mass of the inert gas increases the mean relative velocity v_r of the colliding partners decreases and consequently the duration of the collision τ_c increases. For very heavy inert gas atoms τ_c exceeds the period of spin orbit coupling \hbar/ε . Then the condition:

$$b_{\text{crit}}/v_r = \tau_c = \hbar/\varepsilon \quad (15)$$

(b_{crit} = critical impact parameter)

governs the behaviour of $\sigma_{1/2 \rightarrow 3/2}^{(0)}$ instead of Equation (14).

This explains the decrease of this cross section at the heaviest inert gases. This tendency, however, is not confirmed by quantal calculations of Pascale and Olson [39], who got a continuous increase of $\sigma_{1/2 \rightarrow 3/2}^{(0)}$ from He to Xe (see Table 5).

The numerical values of $\sigma_{1/2 \rightarrow 3/2}^{(1)}$ and $\sigma_{3/2 \rightarrow 1/2}^{(1)}$ in Table 5 agree well with the previous measurements. The negative sign of $\sigma_{j \rightarrow j'}^{(1)}$ indicates that the direction of the polarization ($k=1$) is inverted during the collisional transfer.

The cross sections for the relaxation of the alignment $\sigma_{3/2}^{(2)}$ in Table 5 are at variance with the measurements reported in [20]. The present investigation yields values which are about 20% lower. The increase of the population transfer cross sections between single Zeeman states along with the atomic number of the inert gas atoms (Table 6) gives rise to a respective increase of the cross sections for the relaxation of the $^2P_{3/2}$ tensor components and a decrease of the ratios $\sigma_{3/2}^{(2)}/\sigma_{3/2}^{(1)}$ and $\sigma_{3/2}^{(3)}/\sigma_{3/2}^{(1)}$. In the latter case the increase of $\sigma(3/2, \pm 3/2 \rightarrow 3/2, \mp 3/2)$ plays an important role. It enlarges, namely, $\sigma_{3/2}^{(1)}$ and $\sigma_{3/2}^{(3)}$ and leaves $\sigma_{3/2}^{(2)}$ unchanged. The cross sections $\sigma(1/2, \pm 1/2 \rightarrow 1/2, \mp 1/2)$ in Table 6 agree well with previous measurements reported in [7] and for He, Ne, and Ar with the values published by Niewitecka et al. [31]. However, the great discrepancy for Kr and Xe still demands clarification. The cross sections reported in [31] are measured in zero magnetic fields and are corrected for nuclear spin effects on the basis of the calculations of Franz and Sooriamoorathi [23]. These calculations are performed under the condition:

$$T_c = 1/Nv, \sigma_{1/2}^{(1)*} \gg \tau \quad (16)$$

($\sigma_{1/2}^{(1)*}$ indicates that the authors in [31] applied the definition $\sigma_{1/2}^{(1)*} = 2\sigma(1/2, \pm 1/2 \rightarrow 1/2, \mp 1/2)$ which deviates from the definition of this investigation by $\sigma_{1/2 \rightarrow 3/2}^{(0)}$ (c.f. [20])).

From the directly measured cross sections $\sigma(1/2, \pm 1/2 \rightarrow 1/2, \mp 1/2)$ in Table 6 one deduces, however, that Equation (16) is not valid for the entire pressure range from 0 to 10 Torr as the authors in [31] assert. For Kr and Xe one gets for the higher pressure values $T_c < \tau$. Therefore, we think that the influence of multiple collisions cannot be ignored and that this fact could probably explain the observed discrepancy.

The rapid increase of the cross section $\sigma(3/2, \pm 3/2 \rightarrow 3/2, \mp 3/2)$ in Table 11 is due to the fact that for the heavier inert gases the expectation value of J becomes more and more a good quantum number during the collision process. In the case of He and Ne the relative small value for this cross section indicates that the assumption of decoupled spin and orbital angular momentum during the collision is a justified approximation.

4.3. Comparison of the Present Experimental Results with Theoretical Calculations

Theoretical studies of collision induced fine structure transitions for the system Na-He have been the subject of various publications [29, 30, 33, 34-39].

In Table 7 we compare our results with respective theoretical values. We restrict the comparison to the population transfer cross sections between single Zeeman states. Unfortunately the experimental errors are still too large to decide in favour of a definite theoretical approach. However, it appears [30] that calculations which are done on the base of a semi-empirical potential $V_x - V_H$ given by Nikitin [25] are

Table 7. Comparison between theoretical and the present experimental cross sections for the population transfer between single 2P Zeeman states in the case of Na-inert gas collisions

	Present work 450 K	[33] 400 K	[38] 450 K	[36] ^a 400 K
$\sigma(\frac{1}{2}, \pm \frac{1}{2} \rightarrow \frac{1}{2}, \mp \frac{1}{2})/\text{\AA}^2$	13.2 ± 1.8	14.5 (15.8)	10.7 (11.4)	10
$\sigma(\frac{1}{2}, \pm \frac{1}{2} \rightarrow \frac{3}{2}, \mp \frac{1}{2})/\text{\AA}^2$	31.5 ± 3.9	27.8 (31.4)	25.7 (24.7)	22
$\sigma(\frac{1}{2}, \pm \frac{1}{2} \rightarrow \frac{3}{2}, \pm \frac{1}{2})/\text{\AA}^2$	24.2 ± 3.9	22.2 (23.6)	19.4 (19.0)	17
$\sigma(\frac{3}{2}, \pm \frac{3}{2} \rightarrow \frac{1}{2}, \pm \frac{1}{2})/\text{\AA}^2$	15.8 ± 1.3	16.5 (15.7)	13.2 (13.3)	12
$\sigma(\frac{3}{2}, \pm \frac{3}{2} \rightarrow \frac{1}{2}, \mp \frac{1}{2})/\text{\AA}^2$	35.4 ± 2.3	33.5 (39.2)	32 (30.4)	27
$\sigma(\frac{3}{2}, \pm \frac{3}{2} \rightarrow \frac{3}{2}, \pm \frac{1}{2})/\text{\AA}^2$	28.3 ± 2.4	32.0 (32.0)	25.3 (25.2)	24
$\sigma(\frac{3}{2}, \pm \frac{3}{2} \rightarrow \frac{3}{2}, \mp \frac{1}{2})/\text{\AA}^2$	24.3 ± 2.1	20.6 (19.6)	19.5 (19.1)	18
$\sigma(\frac{3}{2}, \pm \frac{3}{2} \rightarrow \frac{3}{2}, \mp \frac{3}{2})/\text{\AA}^2$	5.6 ± 0.6	5.15 (0)	3.33 (3.21)	3
$\sigma(\frac{3}{2}, \pm \frac{3}{2} \rightarrow \frac{3}{2}, \mp \frac{1}{2})/\text{\AA}^2$	10.8 ± 4.3	20.3 (15.8)	11.0 (11.4)	11

^a These cross sections were calculated by Wilson and Shimoni [38] on the basis of the results of Reid [36]. In brackets the results of other approaches of the authors in [33, 38] are given

Table 8. Grawert parameter [19] $b_1, b_2, b_3, c_1, c_2, b'_1$ for the five inert gases calculated with the values for $\bar{\sigma}(j, \pm m_j \rightarrow j', \pm m'_j)$

	He	Ne	Ar	Kr	Xe
$b_1/\text{\AA}^2$	20 \pm 9	6 \pm 9	23 \pm 12	50 \pm 18	62 \pm 19
$b_2/\text{\AA}^2$	48.0 \pm 6.5	40.6 \pm 6.2	62.6 \pm 11.2	73.2 \pm 13.3	77.0 \pm 13.6
$b_3/\text{\AA}^2$	9.8 \pm 1.1	16.6 \pm 1.4	45.2 \pm 3.2	74.6 \pm 4.6	79.8 \pm 4.8
$c_1/\text{\AA}^2$	13.9 \pm 2.9	12.8 \pm 2.6	16.0 \pm 3.7	18.2 \pm 2.8	20.1 \pm 2.6
$c_2/\text{\AA}^2$	88.5 \pm 5.8	66.8 \pm 4.8	109.0 \pm 7.3	94.0 \pm 5.8	85.5 \pm 5.0
$b'_1/\text{\AA}^2$	19.8 \pm 2.7	21.3 \pm 3.5	44.9 \pm 4.1	96.5 \pm 5.9	108.3 \pm 8.1

in much better agreement than very recent calculations [30] which are done with Pascale and Vandeplanque [40] potentials. Furthermore it is of interest that the more elaborate calculations [33, 38, 36] which consider spin flips during the collision yield values for the cross sections $\sigma(3/2, \pm 3/2 \rightarrow 3/2, \mp 3/2)$ which agree well with the experimental results.

As a first application of the present results we calculated from the cross sections given in Table 4 and 7 the complete set of the parameters $b_1, b_2, b_3, c_1, c_2, b'_1$ introduced by Grawert [19]. In Table 8 these parameters are listed for the five inert gases. The knowledge of the entire Grawert matrix allows one to understand all the processes which include collision induced fine structure transitions for Na $3p^2P$ -inert gas collisions, e.g. optical pumping in the presence of buffer gases, broadening of level crossing signals in low magnetic fields etc.

5. Conclusion

A new method has been reported which allows the measurement of cross sections for the collision induced population transfer between single Na $3p^2P$ Zeeman states. From the optically excited $^2P_{3/2, \pm 3/2}$ or $^2P_{1/2, \pm 1/2}$ states, respectively, we studied the transfer to the other Zeeman states for the magnetic field strengths of 6, 17, 24, and 51 kOe and for the five inert gases. The main influence of the magnetic field could be explained by magnetic mixing of $^2P_{1/2, \pm 1/2}$ and $^2P_{3/2, \pm 3/2}$ states. This effect influences the cross sections $\sigma(j, +m_j \rightarrow j', +m'_j)$ and $\sigma(j, -m_j \rightarrow j', -m'_j)$ in a completely symmetric manner, so that the average of both is free of magnetic mixing effects. Variations of the transfer cross sections due to the changing Zeeman splitting at rising magnetic field are very slight and have only been observed in their tendency for Kr and Xe at the highest field strengths (51 kOe).

Hence, this method allows the determination of cross sections for which the influence of the magnetic field is cancelled. They are therefore particularly suited for the comparison with respective theoretical results and for the calculation of cross sections for the transfer

and the relaxation of the 2P tensor components of the degree 0, 1, 2, and 3.

The results agree well with previous measurements and theoretical calculations. As an application of the present results the non-diagonal elements of Grawerts matrix were deduced.

One of us (W.B.S.) wishes to thank Prof. J. Brossel and Prof. A. Omont for their hospitality and the various suggestions concerning this investigation. The helpful discussions with Prof. M. Elbel during the preparation of this manuscript are also acknowledged. Thanks are due to the Deutsche Forschungsgemeinschaft for financial support.

References

1. Omont, A.: J. Phys. Rad. **26**, 26 (1965)
2. Nikitin, E.E.: Comm. Atom. Molec. Phys. **3**, 7 (1971)
3. Nikitin, E.E.: In: Atomic Physics 4, Proceedings of the 4th International Conference on Atomic Physics 1974, Ed. by G. zu Putlitz, E. W. Weber, A. Winnacker, New York 1975
4. Nikitin, E.E.: In: "The Excited State in Chemical Physics". Ed. by J. Wm. McGowan, New York 1975
5. Omont, A.: Irreducible Components of the Density Matrix: Application to Optical Pumping, to be published in "Progress in Quantum Electronics", 1976
6. Dyakonov, M.I., Perel, V.I.: Soviet Phys. J.E.T.P. **21**, 227 (1965)
7. Schneider, W.B.: Z. Physik **248**, 387 (1971)
8. Berdowski, W., Krause, L.: Phys. Rev. **165**, 158 (1968)
9. Mitchell, A.C.G., Zemansky, M.W.: Resonance Radiation and Excited Atoms, Cambridge Reprint 1961
10. Condon, E.U., Shortley, G.H.: The Theory of Atomic Spectra, Cambridge 1935
11. Williamson, J.H.: Canad. J. Phys. **46**, 1845 (1968)
12. Gay, J.-C., Omont, A.: J. Physique **35**, 9 (1974)
Gay, J.-C.: J. Physique **35**, 813 (1974)
Gay, J.-C.: Thèse d'état, Paris 1976 (unpublished)
13. Gay, J.-C., Schneider, W.B.: J. Physique **36**, L-185 (1975)
Gay, J.-C.: J. Physique **36**, L-239 (1975)
Gay, J.-C., Omont, A.: To be published in J. Physique L (1976)
14. Fuchs, B., Hanle, W., Oberheim, W., Scharmann, A.: Phys. Lett. **50**, 337 (1974)
15. Elbel, M.: Z. Physik **248**, 375 (1971)
16. Elbel, M., Naumann, F.: Z. Physik **20**, 501 (1967); **208**, 104 (1968)
17. Franz, F.A., Franz, J.R.: Phys. Rev. **148**, 82 (1966)
18. Franz, F.A., Shuey, R.T., Leutert, G.: Helv. Phys. Acta **40**, 778 (1967)
19. Grawert, G.: Z. Physik **225**, 283 (1969)
20. Elbel, M., Kamke, B., Schneider, W.B.: Physica **77**, 137 (1974)
21. Elbel, M., Koch, A., Schneider, W.B.: Z. Physik **255**, 14 (1972)

22. Elbel, M., Schneider, W. B.: *Physica* **68**, 146 (1973)
23. Franz, F. A., Sooriarmoorthi, C. E.: *Phys. Rev. A* **8**, 2390 (1973)
24. Pitre, J., Krause, L.: *Canad. J. Phys.* **45**, 2671 (1967)
25. Nikitin, E. E.: *J. Chem. Phys.* **43**, 744 (1965)
26. Dashevskaya, E. I., Nikitin, E. E., Reznikov, A. I.: *J. Chem. Phys.* **53**, 1175 (1970)
27. Dashevskaya, E. I.: *Chem. Phys. Lett.* **11**, 184 (1971)
28. Dashevskaya, E. I., Mokhova, N. A.: *Chem. Phys. Lett.* **20**, 457 (1973)
29. Masnou-Seeuws, F.: *J. Phys. B: Atom. Mol. Phys.* **3**, 1437 (1970)
30. Masnou-Seeuws, F., McCaroll, R.: *J. Phys. B: Atom. Mol. Phys.* **7**, 2230 (1974)
31. Niewitecka, B., Skalinski, T., Krause, L.: *Canad. J. Phys.* **52**, 1956 (1974)
32. Elbel, M., Schneider, W. B.: *Z. Physik* **241**, 244 (1971)
33. Masnou-Seeuws, F., Roueff, E.: *Chem. Phys. Lett.* **16**, 593 (1972)
34. Reid, R. H. G., Dalgarno, A.: *Phys. Rev. Lett.* **22**, 1029 (1969)
35. Reid, R. H. G.: *Chem. Phys. Lett.* **6**, 85 (1970)
36. Reid, R. H. G.: *J. Phys. B: Atom. Molec. Phys.* **6**, 2018 (1973)
37. Lewis, E. L., McNamara, L. F.: *Phys. Rev. A* **5**, 2643 (1972)
38. Wilson, D. A., Shimoni, Y.: *J. Phys. B: Atom. Mol. Phys.* **8**, 2393 (1975)
39. Pascale, J., Olson, R. E.: To be published in *J. Chem. Phys.*
40. Pascale, J., Vandeplanque, J.: *J. Chem. Phys.* **60**, 2278 (1974)
41. Guiry, J., Krause, L.: *Phys. Rev. A* **12**, 2407 (1975)

J.-C. Gay

Laboratoire de Spectroscopie Hertzienne de l'ENS
associé au CNRS (LA No 18) et Université Paris VII
4, Place Jussieu, Tour 12
F-75230 Paris Cedex 05

W. B. Schneider

Fachbereich Physik der Universität Marburg
Renthof 5
D-3550 Marburg 1
Federal Republic of Germany